ADVANCED OPTICAL MATERIALS
www.advopticalmat.de

Helical Stacking Assembly of Orderly Silicon Nanowire Multilayers for Ultrastrong Dissymmetrical Amplification of Circularly Polarized Light

Tai-Ge Dong, Zheng-Guang Wu, Fang-Ling Li, Jun-Zhuan Wang, You-Xuan Zheng, and Lin-Wei Yu**

Circularly polarized organic light-emitting diodes (CP-OLEDs) are ideal candidates to explore novel applications such as 3D displays, optical storage, and quantum computing. However, the low dissymmetry (*g*) factor of most chiral organic materials remains as a major challenge for practical applications. In this work, a helical stacking assembly of orderly silicon nanowires (hs-SiNWs) into a flexible multilayer 3D superstructure is demonstrated to accomplish a strong chiroptical activity. These orderly SiNWs are batch-fabricated via a low temperature in-plane solid–liquid–solid growth mechanism, with precisely-controlled spatial arrangement and mean diameter and length of $D_{nw} = 126 \pm 24$ nm and $L_{nw} > 100$ μm, respectively. To construct such helically-stacked superstructure, the SiNW arrays are transferred and stacked upon transparent glass or flexible polymer substrates, with incremental rotational angle for each layer, which can strongly augment the circularly polarized electroluminescence (CPEL) from conventional CP-OLEDs. Strikingly, the dissymmetry factor increases with more stacking layer up to $g = \pm 0.17$, which is more than 40 times of magnitude higher than that of the original CPEL, among the highest ones reported for CP-OLEDs. These results indicate a promising helical-stacking avenue to boost the chiroptical performance of various CP-OLEDs for scalable and flexible chiroptical applications.

1. Introduction

Circularly polarized light (CPL) is now finding broad applications in optical data storage,[1] quantum computing,[2] bioresponsive imaging,[3] liquid crystal displays,[4] and 3D displays.[5] In pursuit of stronger and yet tunable CPL emission within a relatively simple device architecture, circularly polarized organic light-emitting diodes (CP-OLEDs) have been intensively investigated in the last decade. Various CPL materials have been explored for CP-OLEDs, including conjugated polymers,[5b,6] transition-metal complexes,[7] small organic luminophores,[8] and lanthanide complexes.[9] Although the efficiency has been greatly improved, most of these materials achieve only a rather low dissymmetry (g) factor performance,[10] which is insufficient for practical 3D display and optoelectronic applications.

Among the small organic luminophores, the thermally activated delayed fluorescence (TADF) materials, which could achieve 100% internal quantum efficiency, are considered as a promising choice to construct high-performance chiroptic devices.[11] However, the CP electroluminescence (CPEL) performance of the TADF based CP-OLED is still too low, which restricts their application potentials in practical optoelectronics. Though many efforts have been devoted to developing various chiral materials to boost the performances of CP-OLEDs, a high efficiency electrically driven CPL (or CPEL), with a large *g* factor, still remains a major challenge or bottleneck for practical implementation of CP-OLED applications.

T.-G. Dong, J.-Z. Wang, L.-W. Yu
National Laboratory of Solid State Microstructures/School of Electronics Science and Engineering/Collaborative Innovation Center of Advanced Microstructures
Nanjing University
Nanjing 210093, P. R. China
E-mail: yulinwei@nju.edu.cn

T.-G. Dong
Guangdong-Hong Kong-Macao Joint Laboratory for Intelligent Micro-Nano Optoelectronic Technology/School of Physics and Optoelectronic Engineering
Foshan University
Foshan 528225, P. R. China

Z.-G. Wu, F.-L. Li, Y.-X. Zheng
State Key Laboratory of Coordination Chemistry Collaborative Innovation Center of Advanced Microstructures Jiangsu Key Laboratory of Advanced Organic Materials School of Chemistry and Chemical Engineering
Nanjing University
Nanjing 210023, P. R. China
E-mail: yxzheng@nju.edu.cn

Z.-G. Wu
School of Chemistry and Chemical Engineering
Nantong University
Nantong, Jiangsu 226019, P. R. China

The ORCID identification number(s) for the author(s) of this article can be found under https://doi.org/10.1002/adom.202201105.

DOI: 10.1002/adom.202201105

 © 2022 Wiley-VCH GmbH

In general, the *g* factor, used to characterize the intensity of CP light, is defined as

$$g_{\text{lum}} = 2\times\frac{I_{\text{L}} - I_{\text{R}}}{(I_{\text{L}} + I_{\text{R}})} = 4\times\frac{|m_{ij}||\mu_{ij}|\cos\theta}{|m_{ij}|^2 + |\mu_{ij}|^2} \quad (1)$$

where I_{L} and I_{R} represent the intensities of the left-handed and right-handed CPLs, m_{ij} and μ_{ij} represent the magnetic and electric transition dipole moments (for i→j transition), respectively, and θ denotes the angle between them.[12] A total right- or left-CPL is obtained when *g* values reach either −2 or +2. Under the assumption that only electric and magnetic dipole transitions are considered, Equation (1) can be written as being proportional to the product of $|m_{ij}||\mu_{ij}|$. Because m_{ij} is usually far less than μ_{ij}, most efficient CP-OLED materials can only demonstrate quite low *g* factors.[13] Paradoxically, small electric-dipole transition moment materials can induce large *g* factor, but always have a low luminescence efficiency.[14] Therefore, one should find other strategy to boost the *g* factor for practical CP-OLED applications.

Recently, it has been found that the helical structures are associated with the emission or reflection of strong CPL. For instance, helical stacked microstructures in nature, like the exoskeleton of *C. gloriosa* beetle or the cell walls of the epicarp of *Pollia condensata* fruit, can reflect strongly CPL.[15] In 2015, Cseh et al. fabricated a unique helically stacked arrays composed of Au nanoparticles functionalized with cholesterol liquid crystals,[16] where each stacked layer had a small angle offset from its preceding neighbor layer, and achieved 14 mdeg circular dichroism (CD) response. Then, Tang and co-workers reported in 2017 that 3D nanostructures constructed of helical stacked nanowire (NW) arrays demonstrate a strong CD response.[17] Xu and co-workers fabricated a chiral photonic cellulose film with left-handed periodic helical order and achieved a strong emission of CPL with high *g* value.[18] For the chiral organic materials and CP-OLEDs, the films with helical structures are also investigated for improved *g* factors. Many impressive progresses have been made by Campbell's,[19] Kim's,[20] and Yu's[21] groups in recent years, where rather high g_{EL} factors up to 1.13 is reported, thanks to the formation of the helical structures after annealing treatment of the polymer emitters. Therefore, it is supposed that the helical stacked structures represent an efficient way to amplify the *g* factor of CPEL emission, which is critical for practical applications.

In this work, we propose a 3D helical stacking of orderly planar silicon nanowire (SiNW) array to construct flexible chiral thin film that can strongly magnify the *g* factor of the CPL and CPEL signals of organic TADF materials. The SiNW arrays are grown via an in-plane solid–liquid–solid (IPSLS) mechanism,[22] where the use of amorphous Si (a-Si) thin film as precursor enables a precise guided growth of parallel ultralong SiNWs, in orderly array with predesignable spatial arrangement.[23] Interestingly, the SiNW arrays can be safely transferred and stacked upon transparent glass or polymer substrates, enabling a reliable fabrication of a 3D superstructure consisting of multilayers of helically-stacked Si nanowire (hs-SiNW) arrays, with totally N_{stk} stacking layers and rotation offset angle of $\theta_{\text{rot}} = \pi/N_{\text{stk}}$ between the neighbored layers. Remarkably, this 3D hs-SiNW thin film superstructure can be rather flexible and easily applied to magnify the CP-OLED emission significantly, boosting the initial *g* factor of 4×10^{-3} to a two magnitude higher value of 0.17, which has not been accomplished before.

2. Results and Discussion

Specifically, the SiNW arrays are first grown on SiO_2/c-Si wafer substrates, prepatterned with parallel guiding edge lines, as illustrated schematically in **Figure 1**a. Then, indium (In) catalyst pads/stripes are evaporated, crossing over the guiding edge lines, followed by an H_2 plasma treatment to transform them into discrete In droplets (see Figure 1b). After that, an amorphous Si (a-Si) layer is deposited, prior to an annealing growth in vacuum at 350 °C that activates the In droplets to absorb the a-Si thin film and produce planar SiNWs, which grow along the edges lines as depicted in Figure 1c. More experimental details of the IPSLS growth control are provided in the Experimental Section.

In the next step, a 200 nm thick poly methyl methacrylate (PMMA) thin film is spin-coated over the whole surface, followed by immersing the sample into a diluted HF solution to etch off the underlying SiO_2 layer and release the SiNW array. The released PMMA thin film, holding the SiNWs array (Figure 1e) and floating on the liquid surface, is then picked up and transferred onto quartz plate (Figure 1f). During the placing-stacking process, the stacking number N_{stk} and the rotation offset angle θ_{rot} among the consecutive layers can be precisely controlled. After stacking the multilayers, the PMMA layers can be completely dissolved in air via a 450 °C annealing for 5 min. With the transferring technique, the SiNW array film can also be suspended on the substrated and placed on curve surface (see Figure S2, Supporting Information). The typical as-grown SiNW array are shown in Figure 1g, with a statistic shown in the inset revealing that the SiNW diameters are of $D_{\text{nw}} = 126 \pm 24$ nm. Figure 1h presents a Scanning Electron Microscopy (SEM) image of a 2-layer-stacked SiNW array with a 45° angle offset, lying on wafer surface with regularly controlled orientation and spacing of the ultralong SiNWs (typical length $L_{\text{nw}} > 100$ μm). The atom probe tomography (APT), scanning transmission electron microscopy (STEM), and transmission electron microscopy (TEM) characterizations of the used SiNW had been investigated in our previous work.[22c,23e,24] The alignment quality of the linear nanomaterials is the significant factor in the optical properties of the SiNW array film.[25] By using the IPSLS growth method and the transfer technique, the arrangement of the transferred SiNW array will almost copy the original (see Figure S1, Supporting Information).[23c] More Note that, though the spacing/density of SiNWs in this work has been fixed to be 4 NW μm^{-1}, this density could be further increased to >10 NW μm^{-1}, by using the double or triple-lane guiding edge technology developed in our previous works.[23c,26] In this way, multilayer hs-SiNW thin film, with right- or left-hand-stacking (RHS or LHS) sequences, can be reliably fabricated upon transparent quartz substrate, as seen for example in Figure 1i, where a stack of $N_{\text{stk}} = 10$ layer yellowish RHS-SiNW thin film, with $\theta_{\text{rot}} = 10°$ rotating offset angle, is formed and placed upon a transparent quartz substrate.

© 2022 Wiley-VCH GmbH

21951071, 2022, 23, Downloaded from https://advanced.onlinelibrary.wiley.com/doi/10.1002/adom.202201105 by Nanjing University, Wiley Online Library on [03/11/2026]. See the Terms and Conditions (https://onlinelibrary.wiley.com/terms-and-conditions) on Wiley Online Library for rules of use; OA articles are governed by the applicable Creative Commons License

21951071, 2022, 23, Downloaded from https://advanced.onlinelibrary.wiley.com/doi/10.1002/adom.202201105 by Nanjing University, Wiley Online Library on [03/11/2026]. See the Terms and Conditions (https://onlinelibrary.wiley.com/terms-and-conditions) on Wiley Online Library for rules of use; OA articles are governed by the applicable Creative Commons License

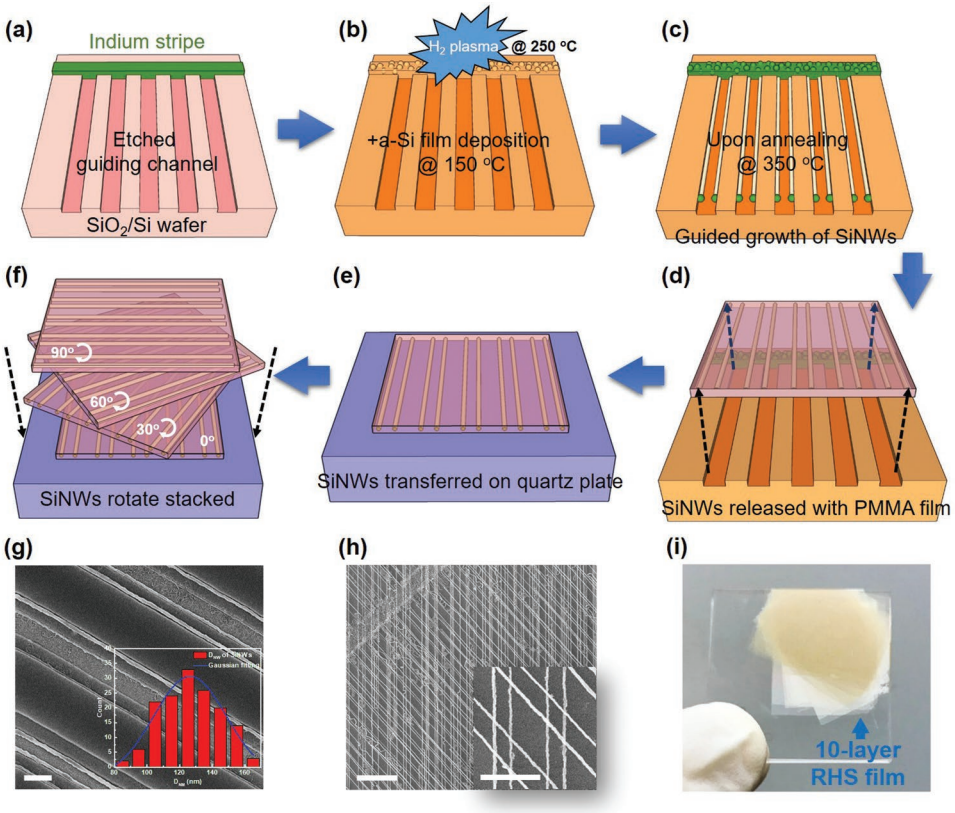


Figure 1. a–c) Schematic diagrams of the fabrication procedures that involve first the patterning of guiding edges patterning and catalyst stripes deposition, a-Si precursor deposition and IPSLS growth of ultralong planar SiNWs. d–f) Depict the layer-by-layer transferring and stacking of the orderly SiNW array onto glass or wafer substrates, repeated for N_{stk} times with a constant rotation offset angle of $\theta_{rot} = 90°/(N_{stk} - 1)$. g) SEM image of the as-grown SiNWs along guiding edge lines, with an inset showing their diameter statistics (Scale bar: 1 µm). h) SEM image of a 45° rotated double layer hs-SiNWs lying on wafer, with an enlarged view of the crossing points provided in the inset, with scale bars of 10 and 2 µm, respectively). i) 10-layer stacked hs-SiNW thin films placed on a transparent quartz substrate, where the rotation offset angle is $\theta_{rot} = 10°$.

Note that, as the chirality of the transmitted light may not be derived from the differential absorption for the left-handed and right-handed light, a Jasco CPL-300 instrument is applied to measure the properties of the hs-films (see the Experimental Section). The CD spectroscopy of the hs-SiNW thin films, with different stacking number and handed sequence, are characterized in an experimental configuration as depicted schematically in **Figure 2**a, where nonpolarized incident lights are introduced to the hs-SiNW thin films from one side, while the polarized transmitted lights are collected and detected on the other side. It is found that the largest CD value and *g* factor are achieved when the total rotation angle, between the last layer and the first layer, is $\theta_{total} = (N_{stk} - 1)\ \theta_{rot} = 90°$. So, in the following study, the interlayer offset angle is always set to $\theta_{rot} = 90°/(N_{stk} - 1)$. In Figure 2b, the CD responses of left-handed hs-SiNW films, with 2, 3, 4, and 10 stacking layers, are presented, indicating that the CD intensity increases substantially with the increase of the inserted stack-layers of N_{stk}, while the corresponding direct current (DC) voltages all peaked at around 0.5 V as seen in Figure 2c. Remarkably, the 10-layer left-handed stacking (LHS) film, the green line in Figure 2a, achieves the largest CD response of 6460 mdeg at 522 nm, which is almost symmetric to the CD of its enantiomer of 10-layer right-handed stacking (RHS) hs-SiNW thin film sample, as witnessed in Figure 2d. The extracted *g* factors for the 10-layer samples are calculated and plotted in Figure 2e, with the largest *g* values of 0.88 and –0.92 achieved at 447 and 459 nm wavelengths for the LHS and RHS configurations, respectively, with a quite wide 60%-bandwidths (BW) of $BW_{60\%} \approx 100$ nm. For comparison, another instrument (Jasco J-1500) is used to measure the CD properties (see Figure S3, Supporting Information). The possible angle dependence effect is estimated (see Figure S4, Supporting Information) and the measurement from the back side or the front side of the film are also tested (see Figure S5, Supporting Information). The calculation of the *g* values is explained in Experimental Section part (Supporting Information). Also, to gain further insight into the chiral mechanism of the 3D hs-nanowire structures, finite element analysis was carried out by using COMSOL simulation toolkits, see Figure S9 (Supporting Information).

For another 10-layer RHS hs-SiNW thin film sample, the highest CD response and thus the *g* factor of –1.17@403 nm has been recorded, as witnessed in **Figure 3**a,b; and Table S1 (Supporting Information), which provides a good platform to testify the macroscopic optical effects of this 3D hs-SiNW superstructure. The green line in Figure 3b indicates that the RH-CP light convert ratio of the nonpolarized incident light is roughly 40–60%. Figure 3c depicts schematically the

 © 2022 Wiley-VCH GmbH

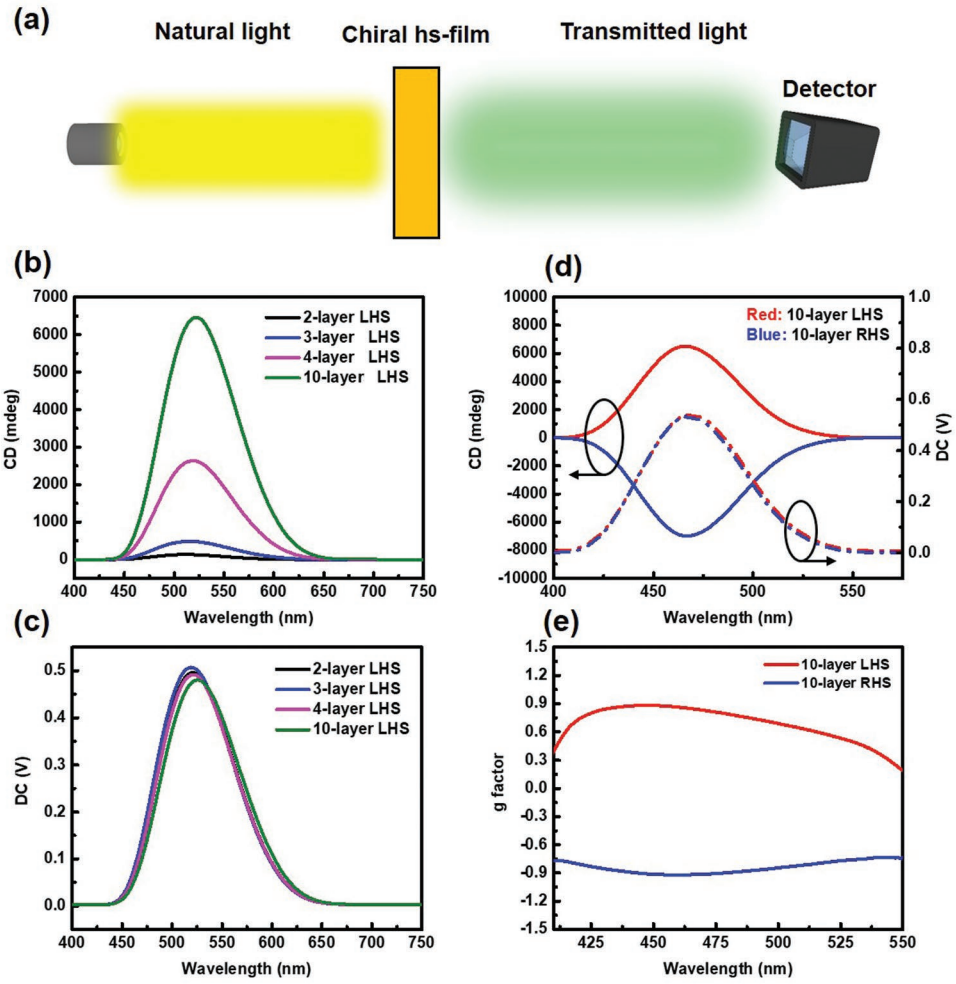


Figure 2. a) Diagram of the experimental setup adopted for the CD response and g factor measurements. b,c) Present the CD responses of the hs-SiNW thin film, with different stacking number but all stacked in LHS sequence, and their corresponding DC voltage readouts, respectively. d) Shows the CD responses and DC voltages of a pair of 10-layer LHS (red) and RHS (blue) hs-SiNW thin films, with the extracted g factors displayed in e).

experimental setup, where the transmitted light is shed in from the left side, passing through first the 10-layer RHS hs-SiNW thin film, and then a circular polarizer film, prior to be seen by the observer on the other side. It is noteworthy that the circular polarizer consists of a right quarter wave plate, which operating wavelength range covers from 400 to 700 nm and 38% transmittance, and a linear polarizer, facing to the observer on the right-hand side. Figure 3d shows the optical image of the maximum brightness of the transmitted light, while the darkest transmitted light is observed when the circular polarizer film is simply rotated over 45°, as seen in Figure 3e.

This observation can be explained as follows: when the polarized light (by the hs-SiNW thin film) travels through the first layer of quarter-wavelength-plate within the circular polarizer, the incident RH-CP light is converted back into linearly polarized status (LP). As a consequence, when the linear polarizer is rotated, the LP can be transmitted or blocked by the second linear polarizer layer, depending on their initial polarization alignment. Specifically, the incident light can be treated as elliptically polarized with a g factor of $|g| < 2$. For the cases that the optical axis of the quarter wave plate is parallel to the long or the short axis direction of the elliptically polarized light, the incident polarized light will be converted back into LP light. Thus, the darkest transmitted light will be observed due to the blocking of the linear polarizer. In other cases, the incident light will not be converted to LP light by the quarter wave plate and thus can be clearly seen by the eyes (not fully blocked). This explains why the transmitted light intensity will vary periodically with every 45° of rotation angle. These results provide a straightforward proof of the strong CP conversion capability of the hs-SiNW film, thanks to the high g factor performance of the unique 3D helically stacked SiNW superstructure.

Furthermore, as one of the most promising application, the hs-SiNW film was incorporated and used as a chiral amplification structure to enhance the CPEL signals, in other words, for achieving a high g factor. For this purpose, a chiral TADF material based CP-OLED, as reported in our previous work with an initial low g_{EL} factor of 4×10^{-3},[27]

© 2022 Wiley-VCH GmbH

21951071, 2022, 23, Downloaded from https://advanced.onlinelibrary.wiley.com/doi/10.1002/adom.202201105 by Nanjing University, Wiley Online Library on [03/11/2026]. See the Terms and Conditions (https://onlinelibrary.wiley.com/terms-and-conditions) on Wiley Online Library for rules of use; OA articles are governed by the applicable Creative Commons License

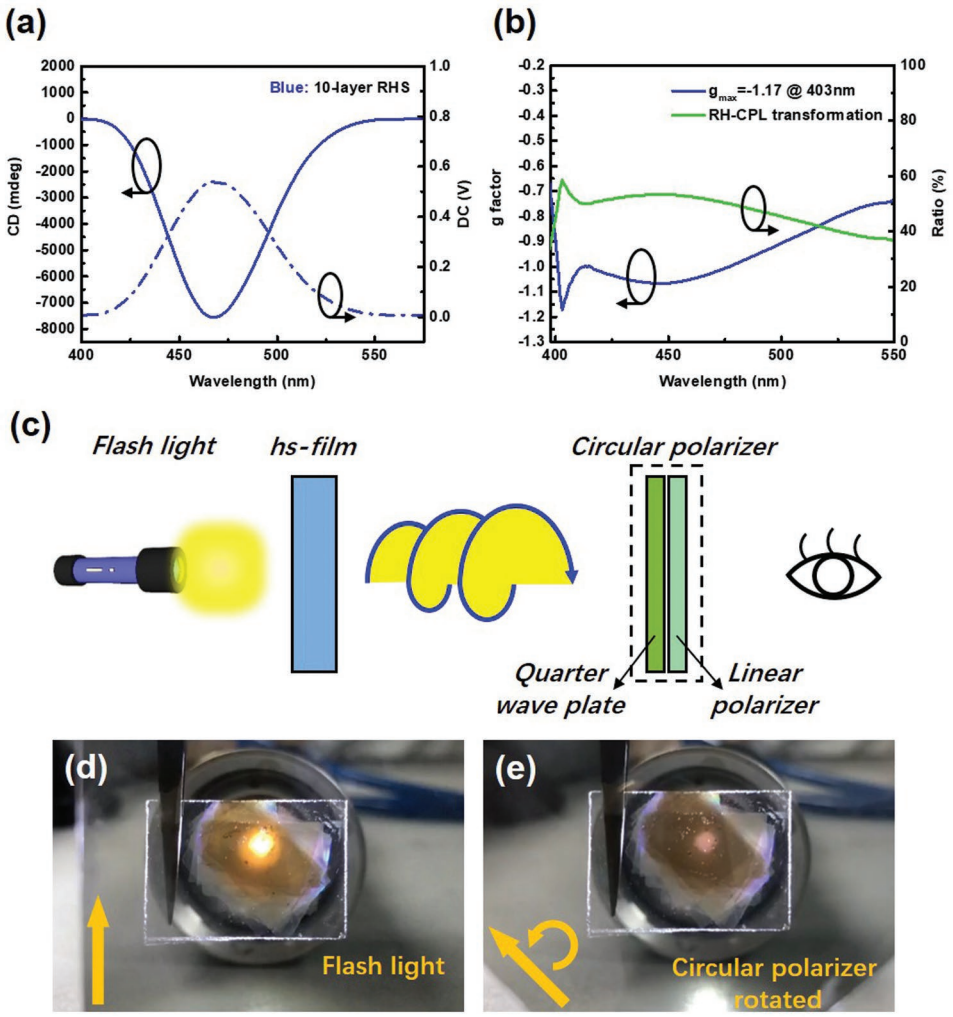


Figure 3. a,b) Shows the CD response and DC voltage spectra of a specific 10-layer RHS hs-SiNW film and the extracted *g* factor (with $g_{max} = -1.17$) at different wavelengths, respectively. c) Diagrams the experimental setup to testify the strong circular polarization effect of the RHS film on an initially unpolarized flash light beam (wavelength range of 400–800 nm). Then, the circularly polarized transmission is passed through a circular polarizer, composed of a quarter wave plate and a linear polarizer, prior to be seen by the observer or camera. d,e) Presents the significant change of transmitted light intensity when rotating the circular polarizer film over 45°, indicating a strong polarization effect, induced by the hs-SiNW film, that can be directly observed by naked eyes.

has been fabricated with a configuration as shown in **Figure 4**a. Remarkably, with the aid of hs-SiNW thin film, the *g* factor of the CPEL emitted from the CP-OLED are greatly magnified by nearly 2 orders (see Figure S7, Supporting Information) and the optical transmittance spectra of the films are shown in Figure S8 (Supporting Information). The TADF enantiomer based CP-OLED, equipped with LHS or RHS hs-SiNW thin film filters, was also investigated, with the corresponding CPEL spectra and the extracted g_{EL} factors shown in Figure 4b,c, respectively, showing a clear enantiomeric relationship. More importantly, the extracted g_{EL} factors can reach as high as 0.17 and –0.17, approaching to practical application requirements in 3D display.[28] The conventional OLEDs with nonpolarized light can also achieve amplified circularly polarized light by combining with the SiNW array film (see Figure S6, Supporting Information), which demonstrates the availability and effectiveness of the SiNW array film in common OLEDs. Thus, these results highlight the unique application potential of the hs-SiNW superstructure.

3. Conclusion

In summary, a 3D helically stacked SiNW multilayer superstructure has been successfully fabricated, for the very first time, where the orderly, slim and ultralong SiNW array were batch-produced via a scalable low-temperature IPSLS growth approach. The flexible hs-SiNW thin films exhibit strong chiral response and rather high *g* factor performance, with the highest values of 0.88 and –0.92 for the LHS and RHS films configurations, respectively. In addition, highly efficient CP-OLEDs, combining TADF enantiomers and the hs-stacked SiNW thin films, demonstrated excellent g_{EL} value of ≈0.17. These results lay a solid basis for constructing a more advanced CP-OLED and have great significance for both academic and industry.

© 2022 Wiley-VCH GmbH

21951071, 2022, 23, Downloaded from https://advanced.onlinelibrary.wiley.com/doi/10.1002/adom.202201105 by Nanjing University, Wiley Online Library on [03/11/2026]. See the Terms and Conditions (https://onlinelibrary.wiley.com/terms-and-conditions) on Wiley Online Library for rules of use; OA articles are governed by the applicable Creative Commons License

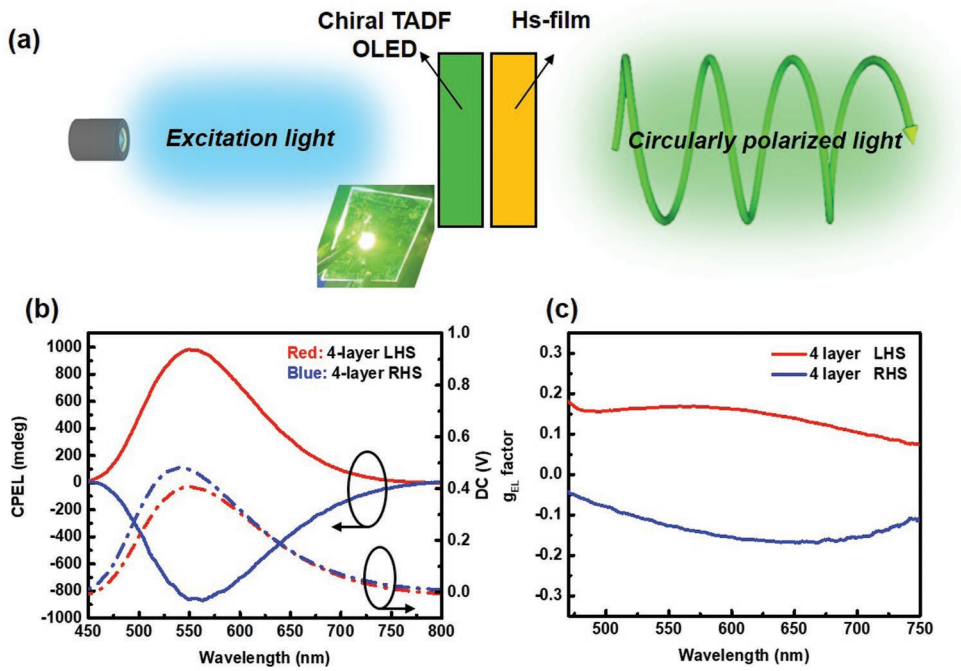


Figure 4. a) Schematics showing the amplification of the *g* factor of a CPL material combing by using the hs-film, while b,c) presents the CPEL and DC voltage spectra of a 4-layer-stacked LHS/RHS films and their corresponding extracted g_{EL} factors.

Supporting Information

Supporting Information is available from the Wiley Online Library or from the author.

Acknowledgements

T.-G.D. and Z.-G.W. contributed equally to this work. The authors acknowledge the financial support received under the National Key Research Program of China under Granted No. 92164201 and National Natural Science Foundation of China under Nos. 11874198, 51773088, and 21975119.

Conflict of Interest

The authors declare no conflict of interest.

Data Availability Statement

The data that support the findings of this study are available from the corresponding author upon reasonable request.

Keywords

3D chiral nanostructure, circularly polarized electroluminescence, dissymmetry factor amplification, organic light-emitting diodes

Received: May 12, 2022
Revised: August 18, 2022
Published online: September 16, 2022

[1] N. Mao, J. Deng, X. Zhang, Y. Tang, M. Jin, Y. Li, X. Liu, K. Li, T. Cao, K. Cheah, H. Wang, J. Ng, G. Li, *Nano Lett.* **2020**, *20*, 7463.
[2] a) P. Lodahl, S. Mahmoodian, S. Stobbe, A. Rauschenbeutel, P. Schneeweiss, J. Volz, H. Pichler, P. Zoller, *Nature* **2017**, *541*, 473; b) B. Lian, X.-Q. Sun, A. Vaezi, X.-L. Qi, S.-C. Zhang, *Proc. Natl. Acad. Sci. USA* **2018**, *115*, 10938.
[3] M. C. Heffern, L. M. Matosziuk, T. J. Meade, *Chem. Rev.* **2014**, *114*, 4496.
[4] a) D. Liu, D. J. Broer, *Langmuir* **2014**, *30*, 13499; b) D. Zhao, H. He, X. Gu, L. Guo, K. S. Wong, J. W. Y. Lam, B. Z. Tang, *Adv. Opt. Mater.* **2016**, *4*, 534.
[5] a) L. Frédéric, A. Desmarchelier, R. Plais, L. Lavnevich, G. Muller, C. Villafuerte, G. Clavier, E. Quesnel, B. Racine, S. Meunier-Della-Gatta, J.-P. Dognon, P. Thuéry, J. Crassous, L. Favereau, G. Pieters, *Adv. Funct. Mater.* **2020**, *30*, 2004838; b) D. Di Nuzzo, C. Kulkarni, B. Zhao, E. Smolinsky, F. Tassinari, S. C. J. Meskers, R. Naaman, E. W. Meijer, R. H. Friend, *ACS Nano* **2017**, *11*, 12713.
[6] a) E. Peeters, M. P. T. Christiaans, R. A. J. Janssen, H. F. M. Schoo, H. P. J. M. Dekkers, E. W. Meijer, *J. Am. Chem. Soc.* **1997**, *119*, 9909; b) Y. Geng, A. Trajkovska, S. W. Culligan, J. J. Ou, H. M. P. Chen, D. Katsis, S. H. Chen, *J. Am. Chem. Soc.* **2003**, *125*, 14032; c) X. Zhang, Y. Zhang, H. Zhang, Y. Quan, Y. Li, Y. Cheng, S. Ye, *Org. Lett.* **2019**, *21*, 439.
[7] a) C. Dee, F. Zinna, W. R. Kitzmann, G. Pescitelli, K. Heinze, L. Di Bari, M. Seitz, *Chem. Commun.* **2019**, *55*, 13078; b) T.-Y. Li, Y.-M. Jing, X. Liu, Y. Zhao, L. Shi, Z. Tang, Y.-X. Zheng, J.-L. Zuo, *Sci. Rep.* **2015**, *5*, 14912.
[8] a) J. Zhao, T. Zhang, X.-Y. Dong, M.-E. Sun, C. Zhang, X. Li, Y. S. Zhao, S.-Q. Zang, *J. Am. Chem. Soc.* **2019**, *141*, 15755; b) S. Feuillastre, M. Pauton, L. Gao, A. Desmarchelier, A. J. Riives, D. Prim, D. Tondelier, B. Geffroy, G. Muller, G. Clavier, G. Pieters, *J. Am. Chem. Soc.* **2016**, *138*, 3990; c) D.-Q. He, H.-Y. Lu, M. Li, C.-F. Chen, *Chem. Commun.* **2017**, *53*, 6093.
[9] a) Y. Hasegawa, M. Yamamuro, Y. Wada, N. Kanehisa, Y. Kai, S. Yanagida, *J. Phys. Chem. A* **2003**, *107*, 1697; b) F. Zinna,

© 2022 Wiley-VCH GmbH

21951071, 2022, 23, Downloaded from https://advanced.onlinelibrary.wiley.com/doi/10.1002/adom.202201105 by Nanjing University, Wiley Online Library on [03/11/2026]. See the Terms and Conditions (https://onlinelibrary.wiley.com/terms-and-conditions) on Wiley Online Library for rules of use; OA articles are governed by the applicable Creative Commons License

U. Giovanella, L. D. Bari, *Adv. Mater.* **2015**, *27*, 1791; c) F. Zinna, M. Pasini, F. Galeotti, C. Botta, L. Di Bari, U. Giovanella, *Adv. Funct. Mater.* **2017**, *27*, 1603719.

[10] a) E. M. Sánchez-Carnerero, A. R. Agarrabeitia, F. Moreno, B. L. Maroto, G. Muller, M. J. Ortiz, S. de la Moya, *Chem. – Eur. J.* **2015**, *21*, 13488; b) H. Tanaka, Y. Inoue, T. Mori, *ChemPhotoChem* **2018**, *2*, 386.

[11] a) F. Ni, C.-W. Huang, Y. Tang, Z. Chen, Y. Wu, S. Xia, X. Cao, J.-H. Hsu, W.-K. Lee, K. Zheng, Z. Huang, C.-C. Wu, C. Yang, *Mater. Horiz.* **2021**, *8*, 547; b) S.-Y. Yang, Y.-K. Wang, C.-C. Peng, Z.-G. Wu, S. Yuan, Y.-J. Yu, H. Li, T.-T. Wang, H.-C. Li, Y.-X. Zheng, Z.-Q. Jiang, L.-S. Liao, *J. Am. Chem. Soc.* **2020**, *142*, 17756; c) Z.-G. Wu, H.-B. Han, Z.-P. Yan, X.-F. Luo, Y. Wang, Y.-X. Zheng, J.-L. Zuo, Y. Pan, *Adv. Mater.* **2019**, *31*, 1900524.

[12] a) J. Han, S. Guo, H. Lu, S. Liu, Q. Zhao, W. Huang, *Adv. Opt. Mater.* **2018**, *6*, 1800538; b) F. S. Richardson, J. P. Riehl, *Chem. Rev.* **1977**, *77*, 773.

[13] F. Zinna, L. Di Bari, *Chirality* **2015**, *27*, 1.

[14] a) G. Longhi, E. Castiglioni, J. Koshoubu, G. Mazzeo, S. Abbate, *Chirality* **2016**, *28*, 696; b) C. K. Luk, F. S. Richardson, *J. Am. Chem. Soc.* **1975**, *97*, 6666.

[15] V. Sharma, M. Crne, O. P. Jung, M. Srinivasarao, *Science* **2009**, *325*, 449.

[16] L. Cseh, X. Mang, X. Zeng, F. Liu, G. H. Mehl, G. Ungar, G. Siligardi, *J. Am. Chem. Soc.* **2015**, *137*, 12736.

[17] J. Lv, K. Hou, D. Ding, D. Wang, B. Han, X. Gao, M. Zhao, L. Shi, J. Guo, Y. Zheng, X. Zhang, C. Lu, L. Huang, W. Huang, Z. Tang, *Angew. Chem., Int. Ed.* **2017**, *56*, 5055.

[18] H. Zheng, W. Li, W. Li, X. Wang, Z. Tang, S. X.-A. Zhang, Y. Xu, *Adv. Mater.* **2018**, *30*, 1705948.

[19] L. Wan, J. Wade, F. Salerno, O. Arteaga, B. Laidlaw, X. Wang, T. Penfold, M. J. Fuchter, A. J. Campbell, *ACS Nano* **2019**, *13*, 8099.

[20] D.-M. Lee, J.-W. Song, Y.-J. Lee, C.-J. Yu, J.-H. Kim, *Adv. Mater.* **2018**, *30*, 1705692.

[21] J.-H. Jung, D.-M. Lee, J.-H. Kim, C.-J. Yu, *J. Mater. Chem. C* **2018**, *6*, 726.

[22] a) L. Yu, P.-J. Alet, G. Picardi, P. Roca i Cabarrocas, *Phys. Rev. Lett.* **2009**, *102*, 125501; b) L. Yu, P. R. i Cabarrocas, *Phys. Rev. B* **2010**, *81*, 085323; c) W. Chen, L. Yu, S. Misra, Z. Fan, P. Pareige, G. Patriarche, S. Bouchoule, P. R. i. Cabarrocas, *Nat. Commun.* **2014**, *5*, 4134; d) M. Xu, Z. Xue, J. Wang, Y. Zhao, Y. Duan, G. Zhu, L. Yu, J. Xu, J. Wang, Y. Shi, K. Chen, P. Roca i Cabarrocas, *Nano Lett.* **2016**, *16*, 7317.

[23] a) L. Yu, M. Oudwan, O. Moustapha, F. Fortuna, P. Roca i Cabarrocas, *Appl. Phys. Lett.* **2009**, *95*, 113106; b) L. Yu, W. Chen, B. O'Donnell, G. Patriarche, S. Bouchoule, P. Pareige, R. Rogel, A. Claire Salaun, L. Pichon, P. Roca i Cabarrocas, *Appl. Phys. Lett.* **2011**, *99*, 203104; c) T. Dong, Y. Sun, Z. Zhu, X. Wu, J. Wang, Y. Shi, J. Xu, K. Chen, L. Yu, *Nano Lett.* **2019**, *19*, 6235; d) H. Ma, R. Yuan, J. Wang, Y. Shi, J. Xu, K. Chen, L. Yu, *Nano Lett.* **2020**, *20*, 5072; e) R. Hu, S. Xu, J. Wang, Y. Shi, J. Xu, K. Chen, L. Yu, *Nano Lett.* **2020**, *20*, 7489.

[24] Z. Xue, M. Sun, T. Dong, Z. Tang, Y. Zhao, J. Wang, X. Wei, L. Yu, Q. Chen, J. Xu, Y. Shi, K. Chen, P. Roca i Cabarrocas, *Nano Lett.* **2017**, *17*, 7638.

[25] a) A. K. Srivastava, W. Zhang, J. Schneider, J. E. Halpert, A. L. Rogach, *Adv. Sci.* **2019**, *6*, 1901345; b) M. F. Prodanov, C. Kang, S. K. Gupta, V. V. Vashchenko, Y. Li, M. Qin, X. Lu, A. K. Srivastava, *Nano Res.* **2022**, *15*, 5392; c) A. K. Srivastava, W. Zhang, J. Schneider, A. L. Rogach, V. G. Chigrinov, H.-S. Kwok, *Adv. Mater.* **2017**, *29*, 1701091.

[26] X. Wu, H. Ma, H. Yin, D. Pan, J. Wang, L. Yu, J. Xu, Y. Shi, K. Chen, *Adv. Electron. Mater.* **2019**, *5*, 1800627.

[27] Z.-L. Tu, Z.-P. Yan, X. Liang, L. Chen, Z.-G. Wu, Y. Wang, Y.-X. Zheng, J.-L. Zuo, Y. Pan, *Adv. Sci.* **2020**, *7*, 2000804.

[28] H. Anetai, T. Takeda, N. Hoshino, Y. Araki, T. Wada, S. Yamamoto, M. Mitsuishi, H. Tsuchida, T. Ogoshi, T. Akutagawa, *J. Phys. Chem. C* **2018**, *122*, 6323.

© 2022 Wiley-VCH GmbH

21951071, 2022, 23, Downloaded from https://advanced.onlinelibrary.wiley.com/doi/10.1002/adom.202201105 by Nanjing University, Wiley Online Library on [03/11/2026]. See the Terms and Conditions (https://onlinelibrary.wiley.com/terms-and-conditions) on Wiley Online Library for rules of use; OA articles are governed by the applicable Creative Commons License